Available online at www.sciencedirect.com
ScienceDirect
International Journal of Heat and Mass Transfer 50 (2007) 3728–3739
International Journal of HEAT and MASS TRANSFER
www.elsevier.com/locate/ijhmt

Improvement of particle concentration prediction in large-eddy simulation by defiltering

B. Shotorban [a], K.K.Q. Zhang [b], F. Mashayek [b,*]

[a] Center for Simulation of Advanced Rockets, University of Illinois at Urbana-Champaign, 1304 West Springfield Avenue, Urbana, IL 61801, United States
[b] Department of Mechanical and Industrial Engineering, University of Illinois at Chicago, 842 West Taylor Street, Chicago, IL 60607, United States

Received 4 January 2007; received in revised form 16 February 2007

Abstract

The main aim of this work is to investigate how reconstructing instantaneous carrier-phase velocities from filtered ones through defiltering improves the prediction of particle concentration in large-eddy simulation (LES) of particle-laden turbulent flows. A particle-laden homogeneous turbulent shear flow is simulated by LES employing the approximate deconvolution method (ADM) to approximate the instantaneous velocities of the carrier phase at the location of particles to solve their Lagrangian momentum equations. The carrier phase is simulated using a Fourier pseudo-spectral method with dynamic Smagorinsky model for subgrid-scale closures. The level of particle concentration is measured by the radial distribution function of particles and the probability density function of the particle number density. Particles with various time constants and terminal velocities are considered and it is shown that employing ADM highly improves the prediction of particle concentration by LES as results are compared against the results obtained by the direct numerical simulation performing *a posteriori* test.

1. Introduction

Considerable progress in the development of accurate models and numerical methods for the large-eddy simulation (LES) of single-phase turbulent flows in the past three decades has encouraged researchers to implement LES for the simulation of two-phase flows in which a large number of particles or droplets (dispersed phase) are carried by a turbulent fluid (carrier) phase. In spite of this progress, there remain conceptual questions on the LES of single-phase flows [1]. In addition, the presence of particles/droplets in the flow raises new questions. Whether various physical features of particle-laden turbulent flows such as preferential accumulation of particles, turbuphoresis, collision and coagulation of particles, and modulation of turbulence by particles can be predicted by LES is still an open question and under investigation.

The common practice in the LES of particle/droplet-laden flows is to individually track particles/droplets through solving their Lagrangian equations while the carrier phase is dealt with in the Eulerian framework and its equations are solved for the filtered quantities. Several studies have been performed through this approach. One of the earliest studies is due to Yeh and Lei [2,3] who investigate the motion of particles in isotropic decaying turbulence and homogeneous shear turbulence. Simonin et al. [4] also study the motion of particles in a homogeneous shear turbulent flow. Wang and Squires [5,6] consider particle-laden fully developed turbulent channel flows while giving particular attention to the preferential accumulation of particles. Uijttewaal and Oliemans [7] simulate turbulence in vertical pipe flows and investigate the particle dispersion and deposition. Boivin et al. [8] study the forced isotropic turbulence in two-way coupling. Yamamoto et al. [9] consider a gas-particle flow in a vertical channel taking into account inter-particle collisions. Apte et al. [10] conduct the LES of swirling particle-laden flows in a coaxial-jet combustor. Also, several works have been

* Corresponding author. Tel.: +1 312 996 1154; fax: +1 312 413 0447.
E-mail address: mashayek@uic.edu (F. Mashayek).

0017-9310/$ - see front matter © 2007 Elsevier Ltd. All rights reserved.
doi:10.1016/j.ijheatmasstransfer.2007.02.033

Nomenclature

B_{ij}	coordinate transformation tensor
C	concentration of particles
C_s	model constant
d_p	particle diameter
f_1	$(1+0.15Re_p^{0.687})$
G	filter kernel
n	locally averaged particle number density
P	instantaneous pressure
p	fluctuating pressure
Re_0	reference Reynolds number
Re_p	particle Reynolds number
S_{ij}	strain rate tensor
$\bar{s}_{ij}$	filtered strain rate
$\bar{u}_i$	filtered fluctuating velocity
U_i	carrier-phase instantaneous velocity
U_{pi}	particle-phase instantaneous velocity
U_{ti}	terminal velocity
U^*_{ti}	terminal velocity non-dimensionalized by Kolmogorov time scale
u_i	carrier-phase fluctuating velocity
$u_i^\star$	reconstructed velocity
u_{pi}	deviation of instantaneous particle velocity from the mean carrier-phase velocity
V_i	Eulerian velocity of particles
x_{pi}	particle position
Greek symbols	
Γ	shear constant
$\overline{\Delta}$	filter size
$\widetilde{\Delta}$	test filter size
$\widetilde{\overline{\Delta}}$	effective filter size
Δ_{DNS}	grid size in DNS
δ_{ij}	Kronecker delta function
ρ	fluid-phase density
ρ_p	particle density
κ	wavenumber
ν	viscosity of the carrier phase
ξ_i	moving coordinate
τ_p	particle time constant
τ^*_p	particle time constant non-dimensionalized by Kolmogorov time scale
τ_{ij}	subgrid stress tensor
τ^d_{ij}	deviatoric part of subgrid stress tensor

conducted for the case of evaporating droplets in mixing layers [11–13] and swirling flows [14].

One of the basic concerns in the LES of particle-laden turbulent flows is how to model the effect of subgrid scales (SGS) on particles. In most works performed in the past, this effect has been neglected and only a few investigations have been carried out with relevance to this issue. Armenio et al. [15] conduct the DNS and LES of a particle-laden turbulent channel flow studying the effect of subgrid scales (SGS) on particles via *a priori* and *a posteriori* tests. They conclude that particles with a small time scale are more influenced by SGS. To the best knowledge of these authors, Wang and Squires [5] are the first investigators who model the effect of SGS on particles. They solve an additional transport equation for the SGS turbulent kinetic energy obtaining a local SGS velocity scale that is used to model this effect through multiplying it by a Gaussian random variable. A similar model is used by Sankaran and Menon [14] to model SGS effect on droplets in swirling flows. Also, stochastic models have been proposed to account for the effect of SGS on particles [16–18].

Recently, defiltering techniques have been implemented to model SGS effects on particles [19–22]. In this approach the instantaneous carrier-phase velocity is reconstructed through defiltering [23] for the use in the dispersed-phase equations. Kuerten and Verman [20] examine the turbophoresis prediction by LES in a turbulent channel flow reconstructing the instantaneous carrier-phase velocities for particles through a defiltering technique in which the filtering inversion is carried out in the Fourier space for the streamwise and spanwise directions while the inversion is approximated by a Taylor series for the cross-stream direction. Shotorban [19] and Shotorban and Mashayek [21] employ the Approximate Deconvolution Method (ADM) of Stolz et al. [24] to reconstruct the instantaneous carrier-phase velocities in particle-laden homogenous turbulent isotropic and shear flows. Most recently Kuerten [22] uses ADM for the reconstruction of carrier-phase velocities to solve the dispersed-phase equations in a channel flow. In all these works it is shown that the prediction of particle related statistics is improved if defiltering is carried out for filtered velocities.

In the current work we study the preferential concentration of particles in the LES of homogenous shear turbulence [25,26] and examine how the use of ADM improves the prediction of preferential concentration. In our previous study [21], it has been briefly shown via *a priori* test, i.e., the results obtained by filtering the DNS velocity field are compared against the DNS results, that this prediction can be improved. In this work, we extend the study in [21] to assess the ADM for particle concentration by conducting *a posteriori* test, i.e., the results obtained by LES are compared against DNS results. In addition, through an asymptotic approach it is proved that the neglect of SGS on particles may result in unphysical concentration of particles. Also, all details about the mathematical formulation as well as the numerical scheme which are not presented in [21] are included in this work. We should mention here that

various physical aspects of particle-laden homogeneous turbulent shear flows have been studied in great details in the past conducting DNS and LES [3,27–30], and our focus in this work is on the concentration of particles in these flows predicted by LES.

In Section 2, we present the governing equations of the particle-laden two-phase flows. In Section 3, the mathematical formulation of homogeneous shear turbulence is given along with LES equations, numerical methodology and overview of simulations. Section 4 is devoted to results and finally, in Section 5, conclusions and discussions are provided.

2. Two-phase flow equations

In the particle-laden flow considered in this study, the carrier phase is an incompressible Newtonian fluid and the dispersed phase is composed of a large number of monodispersed spherical particles of diameter much smaller than the smallest length scale of the carrier-phase flow. It is assumed that the global number density of particles is small and particles can be considered to form a dilute phase. Further, the mass loading is sufficiently small to assume one-way coupling where particles have no effect on the motion of the carrier phase.

2.1. Carrier-phase equations

The carrier phase is governed by the Navier–Stokes equations

$$\frac{\partial U_i}{\partial x_i} = 0, \tag{1}$$

$$\frac{\partial U_i}{\partial t} + U_j \frac{\partial U_i}{\partial x_j} = -\frac{\partial P}{\partial x_i} + \frac{1}{Re_0}\frac{\partial^2 U_i}{\partial x_j \partial x_j}, \tag{2}$$

where U_i is the velocity component in the x_i direction, P is the pressure field and $Re_0 = U_0 L_0/\nu$ is a reference Reynolds number with U_0 and L_0 representing reference velocity and length scales and ν is the fluid viscosity.

2.2. Dispersed-phase equations

Assuming the Stokes drag and gravity to be the only forces acting on the particle, its equations of motion are

$$\frac{\mathrm{d}x_{\mathrm{p}i}}{\mathrm{d}t} = U_{\mathrm{p}i}, \tag{3}$$

$$\frac{\mathrm{d}U_{\mathrm{p}i}}{\mathrm{d}t} = \frac{f_1}{\tau_{\mathrm{p}}}[U_i(\mathbf{x}_{\mathrm{p}}, t) - U_{\mathrm{p}i}] + \frac{U_{\mathrm{t}i}}{\tau_{\mathrm{p}}}, \tag{4}$$

where $\mathbf{x}_{\mathrm{p}} \equiv x_{\mathrm{p}i}$ and $U_{\mathrm{p}i}$ are the instantaneous Lagrangian position and velocity of the particle, respectively. $U_i(\mathbf{x}_{\mathrm{p}}, t)$ denotes the velocity of the carrier phase at the location of the particle. The particle time constant is defined as $\tau_{\mathrm{p}} = Re_0(\rho_{\mathrm{p}}/\rho)d_{\mathrm{p}}^2/18$ where d_{p} is the non-dimensional diameter of the particle and ρ_{p}/ρ is the density ratio of the particle to fluid phase. $f_1 = 1 + 0.15Re_{\mathrm{p}}^{0.687}$ is a correction factor with $Re_{\mathrm{p}} = Re_0|\mathbf{U}(\mathbf{x}_{\mathrm{p}}, t) - \mathbf{U}_{\mathrm{p}}|d_{\mathrm{p}}$. Also, the non-dimensional still fluid terminal velocity of the particle is defined as $U_{\mathrm{t}i} = \tau_{\mathrm{p}} g_i$, where g_i denotes the non-dimensional gravitational acceleration. In general additional forces such as pressure gradient, added mass, buoyancy and Basset history forces must be included on the right-hand side of the particle momentum equation; however, for a high ratio of particle and fluid density, e.g. $\rho_{\mathrm{p}}/\rho = 1000$ considered in this study, and in the absence of walls, these forces can be neglected [31]. This neglect has been justified by Armenio and Fiorotto [32] for a turbulent channel flow.

3. Homogeneous shear turbulence

3.1. Mathematical formulation

In a homogeneous turbulent shear flow, the gradient of the mean velocity is

$$\partial\langle U_i\rangle/\partial x_j = \Gamma\delta_{i1}\delta_{j2}, \tag{5}$$

where Γ is the shear constant and δ_{mn} is the Kronecker delta function. The indices 1 and 2 represent the streamwise x_1 and cross-stream x_2 flow directions, respectively, and $\langle\rangle$ indicates an ensemble average. In the present case of non-stationary homogeneous turbulence, the ensemble average will be replaced by a volume average for the carrier phase. The gradients of all higher order statistical moments of the velocity are zero in homogeneous shear turbulence.

Using $\langle U_i\rangle = \Gamma x_2 \delta_{i1}$ for the mean velocity defined by Eq. (5), the instantaneous velocity field can be decomposed into mean and fluctuation values as

$$U_i = \Gamma x_2 \delta_{i1} + u_i, \tag{6}$$

where u_i is the fluctuation component of the instantaneous velocity. Substituting (6) in Eqs. (1) and (2) results in

$$\frac{\partial u_j}{\partial x_j} = 0, \tag{7}$$

$$\frac{\partial u_i}{\partial t} + \frac{\partial}{\partial x_j}(u_i u_j) + \Gamma\delta_{i1}u_2 + \Gamma x_2 \frac{\partial u_i}{\partial x_1} = -\frac{\partial p}{\partial x_i} + \frac{1}{Re_0}\frac{\partial^2 u_i}{\partial x_j \partial x_j}, \tag{8}$$

which are the governing equations for the carrier-phase velocity and pressure fluctuation components in homogeneous shear turbulence.

Defining $u_{\mathrm{p}i}$ as the deviation of particle instantaneous velocity from the mean velocity of the carrier phase at the location of the particle, i.e.,

$$u_{\mathrm{p}i} = U_{\mathrm{p}i} - \Gamma x_{\mathrm{p}2}\delta_{i1} \tag{9}$$

and substituting for $U_{\mathrm{p}i}$ in Eqs. (3) and (4) results in

$$\frac{\mathrm{d}x_{\mathrm{p}i}}{\mathrm{d}t} = \Gamma x_{\mathrm{p}2}\delta_{i1} + u_{\mathrm{p}i}, \tag{10}$$

$$\frac{\mathrm{d}u_{\mathrm{p}i}}{\mathrm{d}t} = \frac{f_1}{\tau_{\mathrm{p}}}[u_i(\mathbf{x}_{\mathrm{p}}, t) - u_{\mathrm{p}i}(t)] - \Gamma u_{\mathrm{p}2}\delta_{i1} + \frac{U_{\mathrm{t}i}}{\tau_{\mathrm{p}}}. \tag{11}$$

In Eq. (11), $u_i(\mathbf{x}_p, t)$ is the carrier-phase velocity fluctuation at the location of the particle $\mathbf{x}_p$.

3.2. Equations in transformed coordinate system

Periodic boundary conditions are well suited for the simulation of homogeneous turbulence. Nonetheless, periodic boundary conditions cannot be directly applied to solve the governing equations for homogeneous shear turbulence derived in the earlier subsections, because of the appearance of variable coefficients which are functions of x_2 or x_{p2}. This problem can be overcome by using a coordinate system which moves with the mean velocity. This coordinate transformation has been first introduced by Batchelor and Proudman [33] in solving linearized problems of turbulence. Then, Rogallo [34] used the transformation for direct numerical simulation of homogeneous shear turbulence for the first time. More recently, this coordinate transformation was extended to particle-laden turbulent flows by Barre et al. [35].

A coordinate system moving with the mean velocity is defined by

$$\xi_i = B_{ij} x_j, \tag{12}$$

where

$$B_{ij} = \partial \xi_i / \partial x_j = \delta_{ij} - \Gamma t \delta_{i1} \delta_{j2}. \tag{13}$$

Substituting this in Eqs. (7) and (8), we have

$$B_{ji} \partial_j u_i^{\xi} = 0, \tag{14}$$

$$\partial_t u_i^{\xi} + B_{jk} \partial_j (u_i^{\xi} u_k^{\xi}) = -\Gamma u_2^{\xi} \delta_{i1} - B_{ji} \partial_j p^{\xi} + \frac{1}{Re_0} B_{kj} B_{lj} \partial_{kl} u_i^{\xi}, \tag{15}$$

where $\partial_t \equiv \frac{\partial}{\partial t}$, $\partial_j \equiv \frac{\partial}{\partial \xi_j}$, $\partial_{kl} \equiv \frac{\partial^2}{\partial \xi_k \partial \xi_l}$ and the superscript ξ on any field variable denotes that the variable is in the transformed coordinate system. That is

$$u_i^{\xi}(\xi_i, t) = u_i(B_{ij}^{-1} \xi_j, t), \tag{16}$$

where according to (12), $B_{ij}^{-1} \xi_j = x_i$, and u_i^{ξ} is the velocity field described as a function of ξ.

Using (12), particle position is also transformed to the new coordinate

$$\xi_{pi} = B_{ij} x_{pj}, \tag{17}$$

therefore, Eqs. (10) and (11) become

$$\frac{d\xi_{pi}}{dt} = B_{ij} u_{pj}, \tag{18}$$

$$\frac{du_{pi}}{dt} = \frac{f_1}{\tau_p} [u_i^{\xi}(\xi_p, t) - u_{pi}] - \Gamma u_{p2} \delta_{i1} + \frac{U_{ti}}{\tau_p}. \tag{19}$$

3.3. LES formulation

We start with the transformed equations of the homogeneous shear turbulence to derive the LES formulation for the carrier phase. The filtering operator for any field variable in the transformed coordinate is defined in the convolution form as

$$\overline{\Phi}^{\xi}(\xi, t) = G(\xi; \overline{\Delta}) * \Phi^{\xi}(\xi, t) \equiv \int_{-\infty}^{\infty} \Phi^{\xi}(\eta, t) G(\xi - \eta; \overline{\Delta}) \, d^3\eta, \tag{20}$$

where G is the filter kernel function, $*$ is the convolution product operator and $\overline{\Delta}$ is the grid filter size. Applying the filtering operator on Eqs. (14) and (15), results in

$$B_{ji} \partial_j \bar{u}_i = 0, \tag{21}$$

$$\partial_t \bar{u}_i + B_{jk} \partial_j (\bar{u}_i \bar{u}_k) = -\Gamma \bar{u}_2 \delta_{i1} - B_{ji} \partial_j \bar{p} + \frac{1}{Re_0} B_{kj} B_{lj} \partial_{kl} \bar{u}_i - B_{jk} \partial_j \tau_{ik}. \tag{22}$$

For notational convenience, the superscript ξ is suppressed on the filtered variables in Eqs. (21) and (22). In Eq. (22), the subgrid-scale stress tensor is defined as $\tau_{ij} = \overline{u_i u_j} - \bar{u}_i \bar{u}_j$.

Using the Smagorinsky model [36], the deviatoric part of the subgrid-scale stress $\tau_{ij}^d = \tau_{ij} - \tau_{kk} \delta_{ij}/3$ in homogeneous shear turbulence is calculated by

$$\tau_{ij}^d = -2 C_s \overline{\Delta}^2 |\bar{s}| \bar{s}_{ij}, \tag{23}$$

where

$$\bar{s}_{ij} = \frac{1}{2} (B_{kj} \partial_k \bar{u}_i + B_{ki} \partial_k \bar{u}_j) \tag{24}$$

and $|\bar{s}| = (2 \bar{s}_{ij} \bar{s}_{ij})^{1/2}$. The isotropic part $\tau_{kk} \delta_{ij}/3$ is absorbed into the pressure term in Eq. (22) so it is not modeled.

Similar to the procedure introduced by Germano et al. [37] and modified by Lilly [38], the model constant C_s can be dynamically computed

$$C_s = \frac{(m_{ij} l_{ij})_{ave}}{(m_{kl} m_{kl})_{ave}}, \tag{25}$$

where

$$m_{ij} = 2 \overline{\Delta}^2 \widetilde{|\bar{s}| \bar{s}_{ij}} - 2 \widetilde{\overline{\Delta}}^2 |\widetilde{\bar{s}}| \widetilde{\bar{s}}_{ij} \tag{26}$$

and

$$l_{ij} = \widetilde{\bar{u}_i \bar{u}_j} - \widetilde{\bar{u}}_i \widetilde{\bar{u}}_j. \tag{27}$$

In Eqs. (26) and (27), $\tilde{}$ is the filter operator with a test filter size of $\widetilde{\Delta}$. Also in Eq. (27), $\widetilde{\overline{\Delta}}$ is the effective filter size which is equal to $(\overline{\Delta}^2 + \widetilde{\Delta}^2)^{1/2}$ for the Gaussian filter [36]. In this work, the filter is Gaussian and $\widetilde{\Delta} = 2\overline{\Delta}$.

3.4. Approximate deconvolution

Assuming the filter kernel G has an inverse G^{-1}, it can be approximated by the truncated Van Cittert series expansion

$$G^{-1} = \sum_{\alpha=0}^{N} (I - G)^{\alpha}, \tag{28}$$

where I is the identity operator [24]. Employing this equation, the approximate deconvoluted velocity $u_i^\star$ can be computed through consecutively applying the filter

$$u_i^\star = \sum_{\alpha=0}^{N}(1-G)^\alpha * \bar{u}_i = \bar{u}_i + (\bar{u}_i - \bar{\bar{u}}_i) + (\bar{u}_i - 2\bar{\bar{u}}_i + \bar{\bar{\bar{u}}}_i) + \cdots \quad (29)$$

The main advantage of this defiltering technique is that the series expansion can also be used for the filters with compact transfer functions, which are in fact non-invertible, by truncating series and calculating a regularized approximation for the inverse filter kernel [24].

Eq. (29) can be used to approximate the instantaneous velocity of the fluid at the location of the particle required in Eq. (19)

$$u_i^\xi(\xi_p, t) \approx u_i^\star(\xi_p, t). \quad (30)$$

It is noted that only the represented modes of SGS can be reconstructed for the particles by this approximation because any information related to the unrepresented modes is lost in LES.

3.5. Overview of simulations

In this work all DNS and LES simulations are carried out on a $(2\pi)^3$-size box with 128^3- and 64^3-node meshes, respectively. In DNS, the velocity field of the carrier phase is initialized by random numbers with a Gaussian distribution. Moreover, the initial velocity field, which must satisfy the continuity equation, is an isotropic turbulent flow with an energy spectra of $E(\kappa) \propto \kappa^4 \exp(-2\kappa^2/\kappa_m^2)$. Table 1 shows some turbulence parameters of the initial velocity field. The shear constant $\Gamma = 2$ and the reference Reynolds number $Re_0 = 220$ in all simulations. The initial velocity field used in DNS is filtered by a Gaussian filter with $\overline{\Delta} = 4\Delta_{DNS}$, where Δ_{DNS} is the grid size in DNS, and then the filtered initial velocity field is used as the initial condition for the LES simulations. All non-linear convective terms are dealiased by 2/3-rule and phase shift [34,39]. The non-linear SGS stress term in LES is left non-dealiased, because there is no methodology available to remove the aliased errors created by this term. Time advancement is performed using an explicit second-order Adams–Bashforth scheme.

In the homogeneous shear configuration due to the mean velocity gradient the initial isotropic turbulence anisotropically develops in time. In fact, the mean velocity gradient is responsible for turbulence production, and unlike decaying isotropic turbulence here turbulence is maintained. However, in practice, the simulation must be terminated at some time after which the homogeneity assumption breaks down. The reason for the lack of homogeneity in a long run is that, the large scales of turbulence grow in time and the computational domain size at some point in time becomes too small to capture these ever growing scales. In this study, simulations are terminated at $\Gamma t = 8$.

Table 1
Flow parameters for the fluid phase in homogeneous shear turbulence at $\Gamma t = 0$

Re_λ	u_{rms}	κ_m	$\eta\kappa_{max}$	η	τ_η	U_η
24.33	0.4081	7.0	1.674	0.02794	0.1717	0.1627

The coordinate transformation imposed by the mean shear skews the computational grid in time. Consequently, the computation cannot be properly carried out for long time in the highly skewed grid. In order to allow the simulation to progress for a substantial length of time, it is required to remesh the grid periodically to prevent the formation of a highly skewed grid. The procedure of remeshing in homogeneous shear turbulence was first implemented and well explained by Rogallo [34] and in this work, the same remeshing procedure is employed. Remeshing is carried out at $\Gamma t = \frac{1}{2}, \frac{3}{2}, \frac{5}{2}, \ldots$ and the Eulerian variables are interpolated to the new mesh preserving spectral accuracy and making use of periodicity of the computational domain. For more details on the remeshing procedure, readers are referred to [34,19].

In DNS particles are initially randomly distributed throughout the computational domain with a uniform distribution and released with velocities equal to their local fluid velocities. To advance the particles, a second-order Adams–Bashforth scheme is implemented to solve their equations of motion (18) and (19). Also, to compute the velocity of the carrier phase at the location of the particle, i.e., u_i^ξ $(\xi = \xi_p, t)$, a fourth-order Lagrange polynomial interpolation scheme is employed. The accuracy of the interpolation scheme has been tested via comparisons made with the exact values calculated using the fully spectral description [40]. Periodic boundary conditions are applied on particles as well; i.e., when a particle leaves the computational domain from one side, it returns to the domain from the opposite side. Also, the periodicity condition for the particles is used when remeshing is carried out.

In each LES run, three sets of particles are simultaneously followed. For these sets, N is varied from 0 to 2 in Eq. (29) as the instantaneous fluid velocity is reconstructed for particles. These sets are denoted by LES, LES-AD1 and LES-AD2 throughout this work. It is noted that the set with $N = 0$ in Eq. (29) is in fact the one for which the effect of SGS on particles is neglected. All sets of particles are released with an initial velocity equal to their deconvoluted local fluid velocities.

4. Results

In this section we briefly show some results for the carrier phase in the considered homogeneous shear turbulence and give most of the attention to the results obtained for the concentration of particles.

The energy spectra of the filtered velocity $\bar{u}_i$ is shown in Fig. 1. In DNS this spectra is calculated by

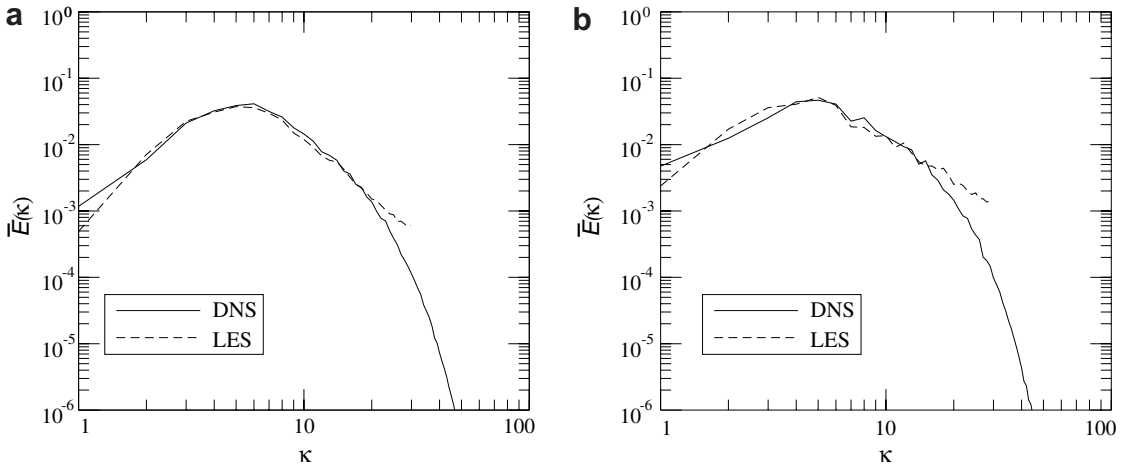

Fig. 1. Energy spectra of the filtered velocity field $\overline{E}$ at (a) $\Gamma t = 3$ and (b) $\Gamma t = 6$.

$\overline{E}(\kappa) = \widehat{G}(\kappa)^2 E(\kappa)$, where $\widehat{G}$ is the Fourier transform of the filter kernel, $E(\kappa)$ is the energy spectra of u_i and κ is the magnitude of the wavenumber vector [36]. Due to the anisotropy of turbulence in the homogeneous shear, various directional velocity energy spectra must be considered; however, in order to briefly demonstrate the accuracy of the LES of the carrier phase, we only consider the variation of the spectrum with the wavenumber magnitude and compare LES to DNS. A detail study of the energy spectra including directional ones in a homogeneous shear turbulent single-phase flow can be found in [34]. As observed in Fig. 1, there is a good agreement between LES and DNS for $\kappa < 20$ at both $\Gamma t = 3$ and $\Gamma t = 6$ but there is a deviation between LES and DNS spectra for $\kappa > 20$. The reason for this deviation is believed to be mainly attributed to the SGS modeling errors.

In order to gain insight into energy balance in the LES of homogeneous shear turbulence, the conservation equation for the kinetic energy of the filtered velocity field $\frac{1}{2}\langle \bar{u}_i \bar{u}_i \rangle$ is considered. This equation can be obtained by multiplying Eq. (22) by $\bar{u}_i$, spatial averaging and using the homogeneousity property. The result can be written as

$$\frac{\partial}{\partial t}\left(\frac{1}{2}\langle \bar{u}_i \bar{u}_i \rangle\right) = -\langle \bar{u}_1 \bar{u}_2 \rangle \Gamma - \overline{\varepsilon} - \varepsilon_{\mathrm{SGS}}, \tag{31}$$

where $\overline{\varepsilon} = B_{kj} B_{lj} \langle \partial_k \bar{u}_i \partial_l \bar{u}_i \rangle / Re_0$ and $\varepsilon_{\mathrm{SGS}} = -\tau^{\mathrm{d}}_{ij} \bar{s}_{ij}$ with τ^{d}_{ij} and $\bar{s}_{ij}$ given in (23) and (24), respectively. Fig. 2 shows the kinetic energy of the filtered velocity field and the terms on the right-hand side of Eq. (31) against the non-dimensional time Γt. There is an initial decay in $\frac{1}{2}\langle \bar{u}_i \bar{u}_i \rangle$ due to the zero value of shear Reynolds stress $\langle \bar{u}_1 \bar{u}_2 \rangle$ at $\Gamma t = 0$ as the initial velocity field is isotropic. This term along with the mean shear velocity gradient Γ is responsible for the production of turbulence which makes $\frac{1}{2}\langle \bar{u}_i \bar{u}_i \rangle$ grow after initial decay period ($\Gamma t < 2$). Comparing $\overline{\varepsilon}$ to $\varepsilon_{\mathrm{SGS}}$, it is seen in Fig. 2 that for $\Gamma t < 0.6$ while $\overline{\varepsilon}$ is almost constant, $\varepsilon_{\mathrm{SGS}}$ rapidly increases in time. This implies that the dissipation of the kinetic energy of the filtered velocity field initially

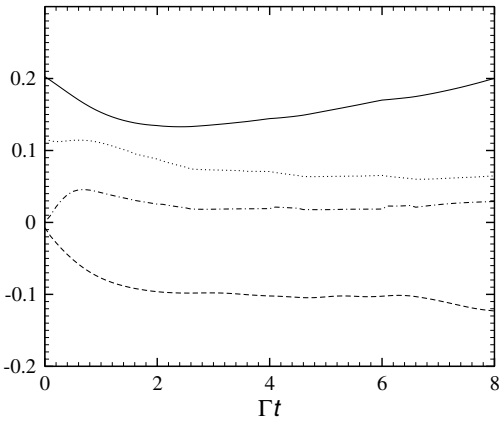

Fig. 2. Energy balance in LES; $\frac{1}{2}\langle \bar{u}_i \bar{u}_i \rangle$ (solid line), $\overline{\varepsilon}$ (dotted line), $\varepsilon_{\mathrm{SGS}}$ (dash-dot line) and $\Gamma \langle \bar{u}_1 \bar{u}_2 \rangle$ (dashed line).

takes place mostly in the resolved scales but as time progresses the role of SGS scales for the dissipation of energy becomes significant. As observed in this figure, more than 2/3 of the energy dissipation takes place in resolved scales through $\overline{\varepsilon}$ and the rest through $\varepsilon_{\mathrm{SGS}}$ for $\Gamma t > 2$.

Time development of particle Reynolds shear stress $\langle\langle u_{\mathrm{p}1} u_{\mathrm{p}2} \rangle\rangle$, with $\langle\langle\rangle\rangle$ denoting ensemble averaging over number of particles, is shown in Fig. 3. Here, $\tau^*_{\mathrm{p}} = \tau_{\mathrm{p}}/\tau_{\eta 0}$ and $U^*_{\mathrm{t}} = U_{\mathrm{t}}/u_{\eta 0}$ with $\tau_{\eta 0}$ and $u_{\eta 0}$ representing the Kolmogorov time and velocity scales, respectively, at $\Gamma t = 0$. The values of Kolmogorov scales are tabulated in Table 1. $\langle\langle u_{\mathrm{p}1} u_{\mathrm{p}2} \rangle\rangle$ is the only non-zero off-diagonal component of the Reynolds stress in the developed homogenous turbulent shear flow [29]. Therefore, it can also be used to measure the level of anisotropy in this flow. As seen in Fig. 3, $\langle\langle u_{\mathrm{p}1} u_{\mathrm{p}2} \rangle\rangle = 0$ at $\Gamma t = 0$ which is due to the uncorrelated initial velocities of the dispersed phase. Then, $\langle\langle u_{\mathrm{p}1} u_{\mathrm{p}2} \rangle\rangle$ develops in time with an almost constant rate until $\Gamma t = 1.5$, after which the development rate of $\langle\langle u_{\mathrm{p}1} u_{\mathrm{p}2} \rangle\rangle$ significantly drops. The development mechanism of particle Reynolds stress in a homogeneous turbulent shear flow is well explained by Mashayek [27]. As seen in Fig. 3, for

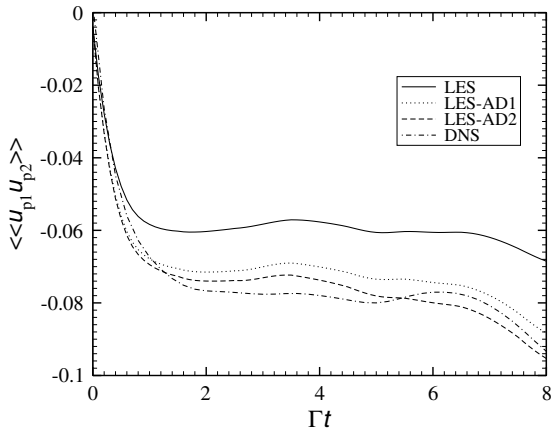

Fig. 3. Time evolution of particle turbulent shear stress $\langle\langle u_{p1}u_{p2}\rangle\rangle$ for $\tau_p^* = 1.165$ and $U_{t1}^* = 0$.

$\Gamma t > 2$ when $\langle\langle u_{p1}u_{p2}\rangle\rangle$ remains almost constant, there is a good agreement between LES-AD1&2 and DNS while LES overpredicts DNS. The overpredication of DNS Reynolds stress by LES is attributed to the decrease of the mean turbulent kinetic energy of the carrier phase which is the result of filtering. In fact, the mean turbulent kinetic energy is the production source for the Reynolds stress in a homogeneous shear turbulent flow [27]. On the other hand, deconvolution is quite able to recover the energy loss due to filtering for the carrier phase.

One of the interesting and important physical features of the particle-laden turbulent flows is the preferential concentration of particles which is the focus of the current study. Particles preferentially accumulate in regions of low vorticity and high strain rate [41,42]. Two quantities can be computed to measure the Lagrangian particle concentration. They are the particle number density (PND) and the radial distribution function (RDF) of particles [43–45,30].

PND is defined as the number of particles in a local unit of volume. In order to calculate this quantity here we use a local averaging technique [46,47] instead of the more traditional box averaging. This methodology was originally introduced for the Eulerian–Eulerian formulation of particle-laden flows, but here we adapt it for the distribution of particles. The local-averaged particle number density, denoted by $n(\mathbf{x}, t)$, is defined as

$$n(\mathbf{x}, t) = \frac{V}{N_p} \sum_{l=1}^{N_p} H(\mathbf{x} - \mathbf{x}_p(t); \delta), \tag{32}$$

where H is the kernel function with the property of

$$\int_{-\infty}^{\infty} H(\mathbf{x}; \delta)\, \mathrm{d}^3\mathbf{x} = 1. \tag{33}$$

Note that the local particle number density is scaled by the global value, N_p/V. In the above equation, δ is the length scale over which local averaging is carried out and N_p is the total number of particles in the whole computational domain. We observe that the spatial variation of the PND computed via this methodology is smoother than binning method. It is emphasized that the larger δ or N_p is, the smoother the spatial variation of the locally averaged PND is. In this study, we take H to be a top-hat function, which is defined by

$$H(\mathbf{x}; \delta) = \begin{cases} 1/\delta^3 & \text{if } |x_i| < \delta/2 \ \forall i = 1, 2, 3, \\ 0 & \text{otherwise.} \end{cases} \tag{34}$$

In the results to be presented, $\delta = 4\Delta_{DNS}$, where Δ_{DNS} is the computational grid size in DNS.

The probability density function (PDF) of n at $\Gamma t = 6$ is presented in Fig. 4 for different cases. The inertialess particles are well mixed in an incompressible flow so they are uniformly distributed. It can be shown that uniformly distributed particles have a Poisson distribution with a peak at $n = 1$ (not plotted in this figure). On the other hand, because of the preferential concentration of inertial particles, their PDF deviates from a Poisson function. In fact, for the inertial particles the PDF broadens as particles are more preferentially accumulated. In other words, due to preferential accumulation of particles the probability of having regions of high and low number densities increases. It is seen in Fig. 4a, b and d for $n > 1.4$, PDF for LES is smaller than that for DNS implying less accumulation of particles in LES. In Fig. 4a the difference between the PDFs for DNS and LES-AD1&2 is insignificant while in Fig. 4b for $n > 2$ the PDF for DNS is slightly overpredicted by LES-AD1&2. In contrast, it is seen in Fig. 4d that for $2 < n < 3$, LES-AD1&2 slightly underpredict DNS. In Fig. 4c, which is for the case with the largest particle time constant studied in this work, it can be seen that for $n < 2.7$ the difference between different curves is small. It is also seen that for all range of n the difference between LES and LES-AD1&2 is negligible in Fig. 4c. This is due to the fact that the effect of small scales of turbulence on particles with large particle time constants is small. It is noted that the difference between the PDFs of DNS, LES and LES-AD1&2 at large n in Fig. 4 may not be a valid base for comparison purposes since at such low values of PDFs the results can be susceptible to statistical noise.

A three-dimensional radial distribution function is defined as the ratio of the number of particle pairs found at a certain separation distance to the expected number if the particles are uniformly distributed [43,45]. The three-dimensional RDF is defined as

$$g_{3D}(r_i) = \frac{P_i/V_i}{P/V}, \tag{35}$$

where $P = N_p(N_p - 1)/2$ is the total number of particle pairs, P_i is the number of pairs within separation distance between $r_i - \Delta r/2$ and $r_i + \Delta r/2$, V is the total volume of the system and $V_i = \frac{4}{3}\pi[(r_i + \Delta r/2)^3 - (r_i - \Delta r/2)^3]$ is the volume of the shell with a thickness of Δr and a radius of r_i at its middle. $\Delta = \Delta_{DNS}/10$ in the results shown in this work.

Fig. 5 presents the 3-D RDF at a fixed time $\Gamma t = 6$ evaluated for particles with different distributions. Here

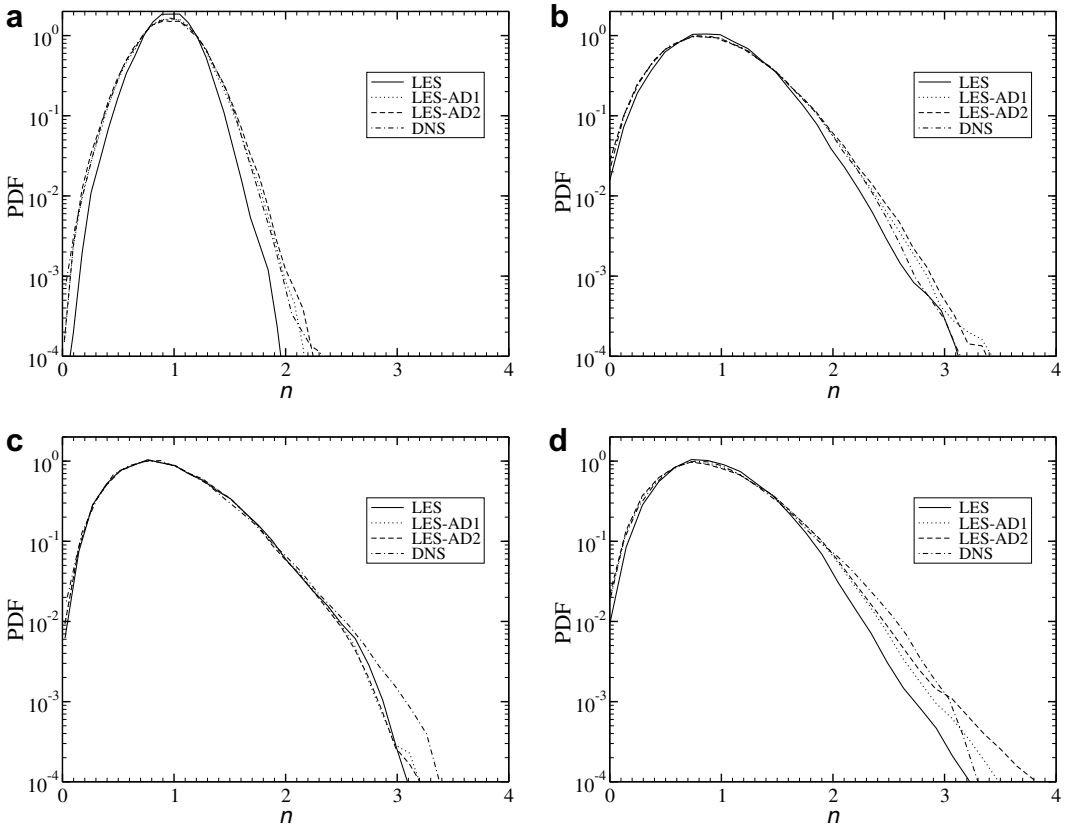

Fig. 4. Probability density function of particle number density at $\Gamma t = 6$; (a) $\tau_p^* = 0.349$ and $U_{tl}^* = 0$; (b) $\tau_p^* = 1.165$ and $U_{tl}^* = 0$; (c) $\tau_p^* = 4.659$ and $U_{tl}^* = 0$; (d) $\tau_p^* = 1.165$ and $U_{tl}^* = 3.245$.

$r^* = r/\eta_0$ with η_0 representing the Kolmogorov length scale at $\Gamma t = 0$. According to the definition of RDF for uniformly distributed particles $g_{3D}(r^*) = 1$ for all r^*. In contrast, in all cases shown in Fig. 5, RDF is greater than 1 for $r^* < 10$, suggesting non-uniform distribution of particles. It is seen in this figure that RDF is a monotonically decreasing function of r^*. In Fig. 5a, b and d RDF for DNS cases is larger than that in LES cases which is another indication that particles are less accumulated in LES. In Fig. 5c there is no significant difference between DNS, LES and LES-AD1&2. This is due to the fact that the effect of SGS on particles with large particle time constants is less critical than that on particles with small particle time constants. In fact, particles with large time constants mainly interact with the large scales of turbulence and the turbulence small scales do not have a large influence on such particles.

Shown in Fig. 6 is the evolution of the 3-D RDF computed by DNS and LES-AD2 for particles with $\tau_p^* = 1.165$ and $U_{tl}^* = 0$. Not plotted in the figure are RDFs at $\Gamma t = 0$ when particles are initially positioned with a uniform random distribution for which the RDF is equal to unity. As Γt increases, RDF increases for small r^* indicating that the number of particle pairs with small separation distance increases. This reveals that the particle accumulation increases as time progresses in a homogeneous shear turbulent flow. A similar observation has been made by Ahmed and Elghobashi [29] who use a different methodology introduced by Wang and Maxey [42] for measuring particle accumulation. It can be seen that LES-AD2 accurately predicts the RDF of DNS at all Γt presented in this figure.

The two-dimensional RDF of particles is defined as

$$g_{2D}(r_i) = \frac{\widetilde{P}_i/A_i}{\widetilde{P}/A}, \tag{36}$$

where $\widetilde{P}$ is the total number of particle pairs in a planner slice of small thickness, $\widetilde{P}_i$ is the number of pairs within the planar slice with separation distances between $r_i - \Delta r/2$ and $r_i + \Delta r/2$, A is the area of the planner slice and $A_i = \pi[(r_i + \Delta r/2)^2 - (r_i - \Delta r/2)^2]$ is the area of the ring associated with the nominal separation distance r_i within the planar slice [45]. In this study, instead of the slicing (binning) method explained by Holtzer and Collins [45] for the calculation of g_{2D}, a slightly different method is employed. Suppose that one needs to compute g_{2D} in slices perpendicular to x_1-axis. Every pair of particles represented by the particle numbers I and J in the domain which satisfies the condition $|x_1^I - x_1^J| \leqslant \delta$ with δ denoting the slice thickness, is considered. Then, $r_i = \sqrt{(x_2^I - x_2^J)^2 + (x_3^I - x_3^J)^2}$ is computed and according to (36), $g_{2D}(r_i)$ is calculated. Note that three different planar RDFs can be computed by choosing mutually

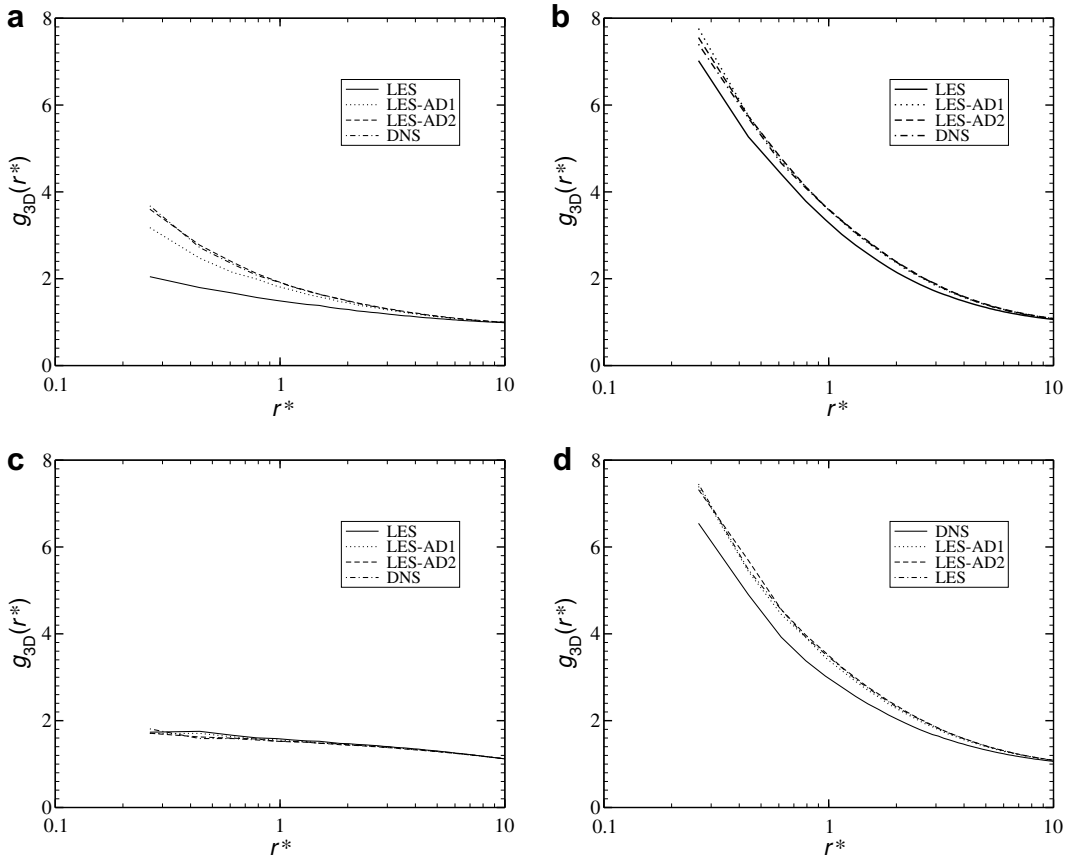

Fig. 5. 3-D radial distribution function of particles at $\Gamma t = 6$; (a) $\tau_p^* = 0.349$ and $U_{t1}^* = 0$; (b) $\tau_p^* = 1.165$ and $U_{t1}^* = 0$; (c) $\tau_p^* = 4.659$ and $U_{t1}^* = 0$; (d) $\tau_p^* = 1.165$ and $U_{t1}^* = 3.245$.

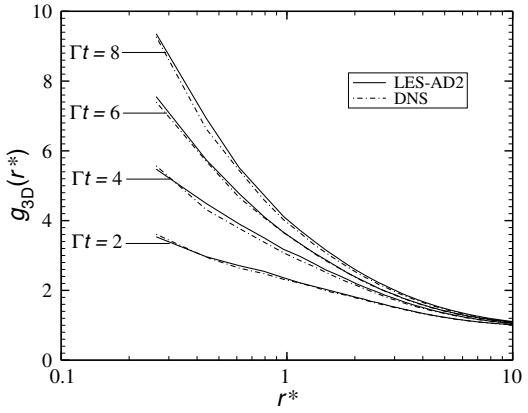

Fig. 6. 3-D radial distribution function of particles at various times for $\tau_p^* = 1.165$ and $U_{t1}^* = 0$.

perpendicular planar slices and here we denote $g_{2D,i}$ to be the two-dimensional RDF with slice perpendicular to x_i direction. The 2-D RDF can be used to measure the anisotropy of the distribution of particles in homogeneous shear turbulence.

The 2-D radial distribution function of particles is displayed in Fig. 7 for $\tau_p^* = 1.165$ and $U_{t1}^* = 0$ at $\Gamma t = 6$. The anisotropic distribution of particles is evident as the 2-D RDFs obtained in different directions are compared. At small r^*s, $g_{2D,1} > g_{2D,3} > g_{2D,2}$ in DNS as well as LES-AD1&2 so particles are the most and the least concentrated in the streamwise and spanwise directions, respectively. It can be seen in this figure that there is a significant difference between DNS and LES while LES-AD1&2 are in a good agreement with DNS. It is also seen that the deviation between LES and DNS cases is the largest for $g_{2D,2}$ while it is the smallest for $g_{2D,1}$.

Now, through an asymptotic approach we investigate the effect of filtering on the concentration of particles. Consider an isotropic turbulent flow that is simulated by LES and effect of SGS on particles is not modeled. In the absence of gravitational force, the particle velocity equation is

$$\frac{\mathrm{d}U_{pi}}{\mathrm{d}t} = \frac{1}{\tau_p}[\overline{U}_i(\mathbf{x}_p, t) - U_{pi}], \tag{37}$$

where $\overline{U}_i(\mathbf{x}_p, t)$ represents the filtered velocity of the carrier phase at the location of the particle. For the sake of simplicity the modified Stokes term f_1 shown in Eq. (4), is not considered here. For a small particle time constant U_p can be expanded as

$$U_{pi} = \overline{U}_i - \tau_p \frac{\overline{DU}_i}{\overline{D}t} + \mathrm{O}(\tau_p^2), \tag{38}$$

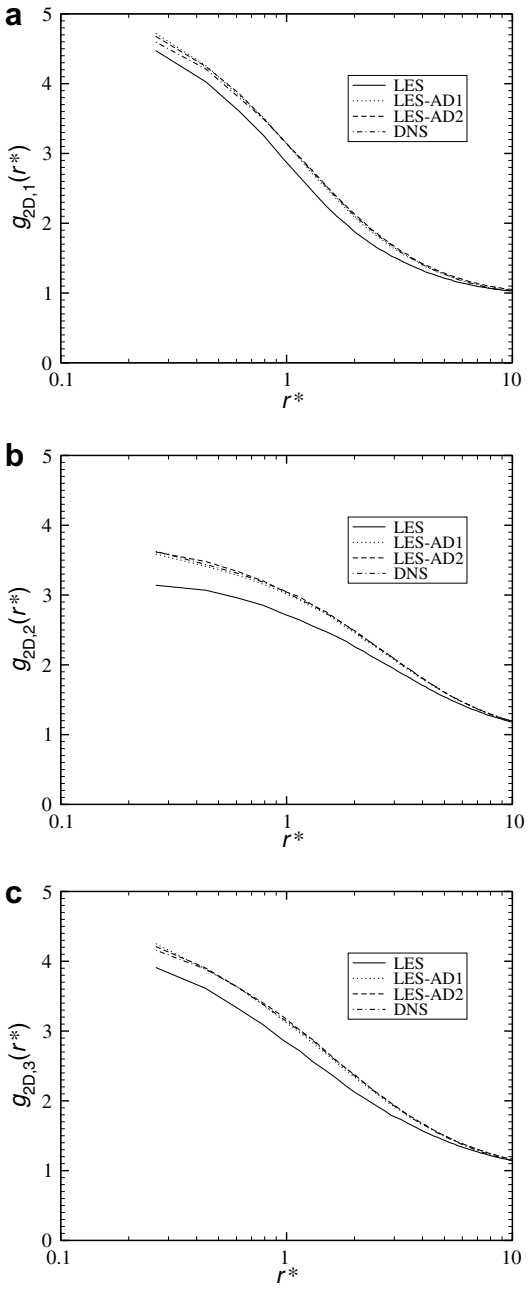

Fig. 7. 2-D radial distribution function of particles for $\tau_p^* = 1.165$ and $U_{tl}^* = 0$ at $\Gamma t = 6$.

where $\overline{\mathrm{D}U}_i/\overline{\mathrm{D}}t = \partial\overline{U}_i + \overline{U}_j\partial\overline{U}_i/\partial x_j$ is the resolved acceleration of fluid at the location of the particle. Eq. (38) is derived through a similar approach provided in Ref. [48] where the particle velocity is expanded in terms of the instantaneous velocity and acceleration of the carrier phase. It is emphasized that Eq. (38) is rigorously valid when $\tau_p \ll T_L$, where T_L is the smallest time scale resolved in LES and associated with the filter size. Also, it should be noted that Eq. (38) is equivalent to approximating the acceleration of the particle with the resolved acceleration of the local fluid for a small particle time constant [49]. This approximation is well justified for $\tau_p/\tau_\eta < 0.4$ in the recent DNS study of Bec et al. [50]. It is noted that the smallest resolved scales are on the order of Kolmogorov scales in DNS while they are on the order of scales associated with the filter size in LES.

Similar to a procedure introduced by Maxey [48], a Eulerian velocity field can be defined for the dispersed phase using (38)

$$V_i = \overline{U}_i - \tau_p \frac{\overline{\mathrm{D}U}_i}{\overline{\mathrm{D}}t}, \tag{39}$$

where V_i is the Eulerian velocity field of the dispersed phase. The divergence of V_i is

$$\frac{\partial V_i}{\partial x_i} = -\tau_p(|\overline{S}|^2 - |\overline{\Omega}|^2), \tag{40}$$

where $|\overline{S}| = (2\overline{S}_{ij}\overline{S}_{ij})^{1/2}$ is the magnitude of the filtered strain rate with $\overline{S}_{ij} = (\partial\overline{U}_i/\partial x_j + \partial\overline{U}_j/\partial x_i)/2$, and $|\overline{\Omega}| = (2\overline{\Omega}_{ij}\overline{\Omega}_{ij})^{1/2}$ is the magnitude of the filtered vorticity with $\overline{\Omega}_{ij} = (\partial\overline{U}_i/\partial x_j - \partial\overline{U}_j/\partial x_i)/2$. Eq. (40) shows that the divergence of the particle velocity field is positive in regions of high filtered vorticity or low filtered strain rate. Therefore, particles tend to accumulate in regions with high filtered strain rates or low filtered vorticities in LES. Again, it is emphasized that Eq. (40) is rigorously valid when $\tau_p \ll T_L$. Now consider a particle time constant satisfying two conditions of $\tau_p \gg \tau_\eta$ and $\tau_p \ll T_L$ and this could be in fact the case for a real LES, in which the filter scales are much larger than the Kolmogorov scales. For a large ratio of particle time constant and Kolmogorov time scale it has been shown that there is no physical accumulation for particles initially released with a uniform distribution. Moreover, the dynamic of the smallest scale, which is basically responsible for the accumulation of finite-inertia particles in isotropic turbulence, cannot accumulate particles with high inertia [42]. In fact, the high inertia of particles makes them move with no correlation to their surrounding fluid. On the other hand, as analytically discussed through an asymptotic approach, accumulation of particles takes place in LES even if $\tau_p \ll T_L$. Therefore, the LES prediction of preferential concentration is in conflict with the physical observation for such particles and modeling SGS effects on them is necessary.

5. Conclusion

Large-eddy simulation (LES) of a particle-laden homogeneous shear turbulent flow is conducted to study preferential concentration of heavy particles in one-way coupling with an incompressible carrier phase. Particles with various time constants and terminal velocities are considered. To model the effect of subgrid scale (SGS) on particles, the instantaneous velocities are reconstructed by approximate deconvolution method (ADM). Preferential concentration of particles is measured by the radial distribution function (RDF) and the probability density function (PDF) of particle number density (PND). In this work the dynamic Smagorinsky model is used as the SGS stress model for the LES of homogeneous shear turbulence. The model is

assessed for this configuration through comparing the energy spectra of the filtered velocities against DNS results.

Carrying out *a posteriori* test, it is observed that the prediction of the preferential concentration by LES is substantially improved for the considered homogeneous turbulent shear flow when the carrier-phase velocities are defiltered for particles. This observation is made possible by comparing the RDF of particles and the PDF of number density of particles obtained by LES against those obtained by DNS for various particle time constants and terminal velocities. It is also observed that the neglect of SGS effects on particles is less critical for particles with a large time constant. This is due to the fact that these particles mainly interact with the large scales of turbulence that are less affected by filtering. Moreover, with the aid of 2-D RDF, the anisotropic concentration of particles in the homogenous shear turbulence is investigated. It is seen that the neglect of subgrid scales is the most and the least critical for particle concentration in cross-stream and streamwise directions, respectively.

It is shown through an asymptotic approach when the SGS effects are neglected on particles in an isotropic turbulent flow, LES may predict an unphysical concentration for them. For a case in which the particle time constant is sufficiently much smaller than the smallest resolved time scale in LES and at the same time it is much larger than the Kolmogorov time scale, it is analytically proven that particles artificially tend to accumulate in the regions with high filtered strain rates and low filtered vorticities if the SGS effect on particles is not modeled. From the standpoint of the flow physics, there must not occur any concentration for particle time constants that are much larger than the Kolmogorov time scale.

Acknowledgments

The Center for Simulation of Advanced Rockets is supported by the US Department of Energy through the University of California under Subcontract No. B523819. Partial support for this work was provided by the Office of Naval Research under grant N00014-05-1-0253.

References

[1] S.B. Pope, Ten questions concerning the large-eddy simulation of turbulent flows, New J. Phys. 6 (2004). Art. No. 35.
[2] F. Yeh, U. Lei, On the motion of small particles in a homogeneous isotropic turbulent flow, Phys. Fluids 3 (11) (1991) 2571–2586.
[3] F. Yeh, U. Lei, On the motion of small particles in a homogeneous turbulent shear flow, Phys. Fluids 3 (11) (1991) 2758–2776.
[4] O. Simonin, E. Deutsch, M. Boivin, Large eddy simulation and second-moment closure model of particle fluctuating motion in two-phase turbulent shear flows, in: F. Durst, N. Kasagi, B. Launder, F. Schmidt, J. Whitelaw (Eds.), Turbulent Shear Flows, vol. 9, Springer-Verlag, 1995, pp. 85–115.
[5] Q. Wang, K.D. Squires, Large eddy simulation of particle-laden turbulent channel flow, Phys. Fluids 8 (5) (1996) 1207–1223.
[6] Q. Wang, K. Squires, Large eddy simulation of particle deposition in a vertical turbulent channel flow, Int. J. Multiphase Flow 22 (4) (1996) 667–683.
[7] W. Uijttewaal, R. Oliemans, Particle dispersion and deposition in direct numerical simulation and large eddy simulations of vertical pipe flows, Phys. Fluids 8 (1996) 2590–2604.
[8] M. Boivin, O. Simonin, K.D. Squires, On the prediction of gas–solid flows with two-way coupling using large eddy simulation, Phys. Fluids 12 (2000) 2080–2090.
[9] Y. Yamamoto, M. Potthoff, T. Tanaka, T. Kajishima, Y. Tsuji, Large-eddy simulation of turbulent gas-particle flow in a vertical channel: effect of considering inter-particle collisions, J. Fluid Mech. 442 (2001) 303–334.
[10] S. Apte, K. Mahesh, P. Moin, J. Oefeleini, Large-eddy simulation of swirling particle-laden flows in a coaxial-jet combustor, Int. J. Multiphase Flow 29 (8) (2003) 1311–1331.
[11] N. Okong'o, J. Bellan, A priori subgrid analysis of temporal mixing layers with evaporating droplets, Phys. Fluids 12 (6) (2000) 1573–1591.
[12] N. Okong'o, J. Bellan, Consistent large-eddy simulation of a temporal mixing layer laden with evaporating drops. Part 1. Direct numerical simulation formulation and a priori analysis, J. Fluid Mech. 499 (2004) 1–47.
[13] A. Leboissetier, N. Okong'o, J. Bellan, Consistent large-eddy simulation of a temporal mixing layer laden with evaporating drops. Part 2. A posteriori modelling, J. Fluid Mech. 523 (2005) 37–78.
[14] V. Sankaran, S. Menon, LES of spray combustion in swirling flows, J. Turbul. 3 (2002). Art. No. 11.
[15] V. Armenio, U. Piomelli, V. Fiorotto, Effect of the subgrid scales on particles motion, Phys. Fluids 11 (1999) 3030–3042.
[16] B. Shotorban, F. Mashayek, A stochastic model for particle motion in large-eddy simulation, J. Turbul. 7 (2006). Art. No. 18.
[17] I. Vinkovic, C. Aguirre, S. Simoens, M. Gorokhovski, Large eddy simulation of droplet dispersion for inhomogeneous turbulent wall flow, Int. J. Multiphase Flow 17 (2006). Art. No. 112101.
[18] A. Elhami Amiri, S. Kazemzadeh Hannani, F. Mashayek, Large-eddy simulation of heavy-particle transport in turbulent channel flow, Numer. Heat Transfer Part B 50 (2006) 285–313.
[19] B. Shotorban, Modeling of subgrid-scale effects on particles in large-eddy simulation of turbulent two-phase flows, Ph.D. thesis, University of Illinois at Chicago, Chicago, IL, 2005.
[20] J.G.M. Kuerten, A.W. Verman, Can turbuphoresis be predicted by large-eddy simulation? Phys. Fluids 17 (2005). Art. No. 011701.
[21] B. Shotorban, F. Mashayek, Modeling subgrid-scale effects on particles by approximate deconvolution, Phys. Fluids 17 (2005). Art. No. 081701.
[22] J.G.M. Kuerten, Subgrid modeling in particle-laden channel flow, Phys. Fluids 18 (2006). Art. No. 025108.
[23] P. Sagaut, Large Eddy Simulation for Incompressible Flows: An Introduction, second ed., Springer Verlag, Berlin, Germany, 2002.
[24] S. Stolz, N.A. Adams, L. Kleiser, An approximate deconvolution for large-eddy simulation with application to incompressible wall-bounded flows, Phys. Fluids 13 (4) (2001) 997–1015.
[25] J. Bardina, J.H. Ferziger, W.C. Reynolds, Improved turbulence models based on large eddy simulations of homogeneous, incompressible, turbulent flows, Department of Mechanical Engineering Report TF-19, Stanford University, Stanford, CA, 1983.
[26] Y. Wang, F.G. Jacobitz, C.J. Rutland, Application of the large-eddy approach to the simulation of turbulence in uniform shear flow, Numer. Heat Transfer Part B 48 (2005) 499–516.
[27] F. Mashayek, Droplet-turbulence interactions in low-Mach-number homogeneous shear two-phase flows, J. Fluid Mech. 367 (1998) 163–203.
[28] A.M. Ahmed, S. Elghobashi, On the mechanism of modifying the structure of turbulent homogeneous shear flows by dispersed particles, Phys. Fluids 12 (2000) 2906–2930.
[29] A.M. Ahmed, S. Elghobashi, Direct numerical simulation of particle dispersion in homogeneous turbulent shear flows, Phys. Fluids 13 (2001) 3346–3364.
[30] B. Shotorban, S. Balachandar, Particle concentration in homogeneous shear turbulence simulated via Lagrangian and equilibrium Eulerian approaches, Phys. Fluids 18 (2006). Art. No. 065105.

[31] M.R. Maxey, J.J. Riley, Equation of motion for a small rigid sphere in a nonuniform flow, Phys. Fluids 26 (1983) 883–889.
[32] V. Armenio, V. Fiorotto, The importance of the forces acting on particles in turbulent flows, Phys. Fluids 13 (2001) 2437–2440.
[33] G.K. Batchelor, I. Proudman, The large-scale structure of homogeneous turbulence, Phil. Trans. Roy. Soc. Lond. 248 (949) (1956) 46–405.
[34] R.S. Rogallo, Numerical experiments in homogeneous turbulence, Tech. Rep. 81315, NASA TM, 1981.
[35] C. Barré, F. Mashayek, D.B. Taulbee, Statistics in particle-laden plane strain turbulence by direct numerical simulation, Int. J. Multiphase Flow 27 (2) (2001) 347–378.
[36] S.B. Pope, Turbulent Flows, Cambridge University Press, Cambridge, UK, 2000.
[37] M. Germano, U. Piomelli, P. Moin, W.H. Cabot, A dynamic subgrid-scale eddy viscosity model, Phys. Fluids A 3 (7) (1991) 1760–1765.
[38] D.K. Lilly, A proposed modification of the Germano subgrid-scale closure method, Phys. Fluids A 4 (3) (1992) 633–634.
[39] C. Canuto, M.Y. Hussaini, A. Quarteroni, T.A. Zang, Spectral Methods in Fluid Dynamics, Springer-Verlag, New York, NY, 1987.
[40] B. Balachandar, M.R. Maxey, Methods for evaluating fluid velocities in spectral simulations of turbulence, J. Comp. Phys. 83 (1989) 96–125.
[41] K.D. Squires, J.K. Eaton, Preferential concentration of particles by turbulence, Phys. Fluids 3 (5) (1991) 1169–1178.
[42] L.-P. Wang, M.R. Maxey, Settling velocity and concentration distribution of heavy particles in isotropic turbulence, J. Fluid Mech. 256 (1993) 27–68.
[43] W.C. Reade, L.R. Collins, A numerical study of the particle size distribution of an aerosol undergoing turbulent coagulation, J. Fluid Mech. 415 (2000) 45–64.
[44] R.C. Hogan, J.N. Cuzzi, Stokes and Reynolds number dependence of preferential particle concentration in simulated three-dimensional turbulence, Phys. Fluids 13 (2001) 2938–2945.
[45] G.L. Holtzer, L.R. Collins, Relationship between the intrinsic radial distribution function for an isotropic field of particles and lower-dimensional measurements, J. Fluid Mech. 459 (2002) 93–102.
[46] T.B. Anderson, R. Jackson, A fluid mechanical description of fluidized beds, Ind. Eng. Chem. Fund. 6 (1967) 527–539.
[47] R. Jackson, Locally averaged equations of motion for a mixture of identical spherical particles and a Newtonian fluid, Chem. Eng. Sci. 52 (15) (1997) 2457–2469.
[48] M.R. Maxey, The gravitational settling of aerosol particles in homogeneous turbulence and random flow fields, J. Fluid Mech. 174 (1987) 441–465.
[49] J. Ferry, S. Balachandar, A fast Eulerian method for disperse two-phase flow, Int. J. Multiphase Flow 27 (7) (2001) 1199–1226.
[50] J. Bec, L. Biferale, G. Boffetta, A. Celani, M. Cencini, A. Lanotte, S. Musacchio, F. Toschi, Acceleration statistics of heavy particles in turbulence, J. Fluid Mech. 550 (2006) 349–358.